Met. Mater. Int., Vol. 22, No. 2 (2016), pp. 216~221
doi: 10.1007/s12540-016-5478-y

Effect of Final Heat Treatment on Creep Behaviors of Zr-Nb-Cu Alloy Cladding Tubes

In Won Kim and Sun Ig Hong*

Department of Advanced Materials Engineering, Chungnam National University, Daejeon 305-764, Korea

(received date: 2 September 2015 / accepted date: 7 December 2015)

Creep properties of annealed and stress-relieved Zr-1.1Nb-0.05Cu cladding tubes were studied and compared. The creep rates of Zr-1.1Nb-0.05Cu cladding tubes stress-relieved at 560 ℃ were found to be appreciably higher than those of Zr-1.1Nb-0.05Cu annealed at 700 ℃. The stress exponents for steady state creep were observed to be 5.0~7.0 for both stress-relieved and annealed Zr-1Nb-0.05Cu, supporting that the dislocation-climb-controlled creep operates at the intermediate temperatures (450~500 ℃). The creep activation energy increased appreciably in the annealed Zr-1.1Nb-0.05Cu alloy compared to those of stress-relieved alloy. The increase of activation energy in the annealed Zr-1.1Nb-0.05Cu alloy is attributed to the decreasing contribution of faster diffusion path such as grain boundaries and dislocations. The creep rate of Zr-1.1Nb-0.05Cu decreased at intermediate temperatures with the increase of grain size with heat treatment, supporting the creep performance can be improved by the modification of microstructure through annealing.

Keywords: creep rate, creep life, cladding, fracture, Zr-1.1Nb-0.05Cu

1. INTRODUCTION

Zr alloy claddings play important roles not only as the barrier material that prevents nuclear fission products from being released into the circulating cooling water, but also as the conducting material that transfers fission-generated heat readily to the cooling water. To ensure the integrity and safety of nuclear fuels and nuclear reactors [1-8], creep properties of Zr cladding tubes at the intermediate and high temperatures should meet the requirement. The corrosion resistance is also one of the most important performance requirements for nuclear reactor reliability. Nuclear claddings should withstand the local stress caused by the pellet-clad mechanical interaction (PCMI) acting on the inner surface of claddings as well as the stress resulting from the pressurized coolant acting on the outer surface in the corrosive environment [2].

Zr-Nb based alloys have been used as nuclear fuel claddings in nuclear power reactors because of their excellent corrosion resistance [1,2] and good mechanical properties. The in-reactor performance evaluations of various Zr alloys have shown that Nb increases not only corrosion and radiation-induced growth (volume conservative distortion) [4] resistance but also creep resistance. The efficiency of Zr alloy claddings can be modified by the modification of alloying elements as well as by modification of thermo-mechanical processing schedules. The microstructural details of Zr alloy claddings including the dislocation density, the grain size, the texture and the shape, distribution and size of second phase particles are greatly influenced by the accumulation of the strain energy by room temperature pilgering and the release of it by heat treatment.

Post-cold-pilgering heat treatment of Zr alloy claddings is known to decrease the tensile strength, but to enhance the resistances to corrosion and irradiation-induced growth [5]. Some Zr alloy tube manufacturers heat-treat cladding tubes under the stress relieved condition to enhance the strength and creep properties whereas other manufacturers heat-treat the cladding tubes under the recrystallized condition to improve the corrosion resistance properties and irradiation growth resistance. It has been suggested that the creep and mechanical properties can be modified not only by the modification of alloy composition, but also by the modification of grain size in Zr alloys [5,9,10]. In the present study, the influence of heat treatment on the grain growth and the creep performance of Zr-1.1Nb-0.05Cu claddings were investigated.

2. EXPERIMENTAL PROCEDURES

In the present study, Zr-1.1Nb-0.05Cu alloy cladding tubes were fabricated by room temperature pilgering with double intermediate heat treatments and post-pilgering stress-relief treatment at 560 ℃ for 5 hrs. To increase the grain size, some Zr-1.1Nb-0.05Cu alloy cladding tubes were further heat-

*Corresponding author: sihong@cnu.ac.kr

treated at 700 °C for 3 h in argon atmosphere. The experimental samples additionally annealed at 700 °C after stress-relief treatment will be called "annealed" samples. To investigate the circumferential creep behaviors of Zr-1.1Nb-0.05Cu alloy cladding tubes, the Zr alloy tubes were sectioned perpendicularly to the tube axis of cladding tubes by the width of 4 mm. In this study, a set of specially designed grips with two half-cylinders was used to strain the Zr-1.1Nb-0.05Cu alloy cladding tube specimen circumferentially while keeping a round shape of the ring specimens in contact with the specially designed grips [1,2,11,12]. Constant stress creep testing machines with the loading cam profile designed to maintain the constant stress in the creep-straining specimens were used to examine the influence of grain size on creep performance and properties. The constant stress creep experiments were carried out in the applied stress and temperature ranges of 80 MPa~120 MPa and 450 °C~500 °C, respectively.

For microstructural and nano-structural analyses, transmission electron microscopy (TEM) specimens were prepared from the stress-relieved and annealed specimens. Using a twin jet polisher with the perchloric acid (10%)-ethanhol solution in the temperature of -35 to -45 °C, 3 mm disks were electro-polished until perforation in the 3 mm disk with the voltage of 12-20 V. TEM specimens were examined by a TEM (JEOL-2010) equipped with an energy dispersive X-ray spectroscopy (EDS) detector with an accelerated voltage of 200 kV. For fracture surface analyses, scanning electron microscopy (SEM) were performed using a JEOL JSM-7000F.

3. RESULT AND DISCUSSION

Typical TEM microstructure of the stress-relieved (a) and annealed (b) Zr-1.1Nb-0.05Cu claddings showing the grain morphology are exhibited in Fig. 1. The Zr-1.1Nb-0.05Cu cladding tubes with stress-relief heat treatment showed numerous equi-axed grains with dislocations and small round particles. In Zr-1.1Nb-0.05Cu alloy cladding tubes with annealing, large recrystallized grains and the rod-shaped particles in the recrystallized grains were observed. The dislocation density in the stress-relieved Zr-1.1Nb-0.05Cu alloy cladding tubes was observed to be higher. The grain size of Zr-1.1Nb-0.05Cu tubes with stress-relief heat treatment was observed to be 0.9~1.2 μm, and that of annealed Zr-1.1Nb-0.05Cu was found to be 4.0~5.0 μm. The grain size was measured using a linear intercept method. Zr alloy cladding tubes generally have strong radial texture, which was thought to have strength and suppress delayed hydride cracking [11,12]. The radial texture developed during pilgering process is not known to be greatly modified by annealing [11,12].

In the stress-relieved alloy in Fig. 1(a), small round-shaped precipitates were observed mostly in the grain interior (some of them indicated by white arrows) and elongated second phase (marked with "S") was observed at grain boundaries.

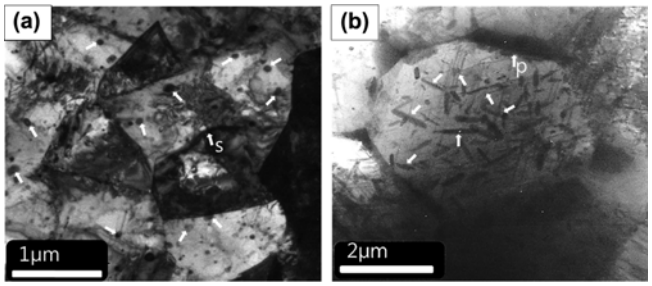

Fig. 1. Typical TEM microstructure of the stress-relieved (a) and annealed (b) Zr-1.1Nb-0.05Cu cladding tubes showing the grain morphology.

The round precipitates and elongated second phase in Zr-1Nb alloy heat-treated below the monotectoid temperature were identified to be $Zr(NbFe)_2$ and β_{Nb} phase, respectively, using selected area diffraction (SAD) analysis by Jeong *et al*. [6]. In the annealed alloy in Fig. 1(b), small rod-shaped precipitates were observed in the grain interior (indicated by white arrows) as well as elongated plate-type second phase (marked with "P") at grain boundaries. Jeong *et al.* [6] also reported that rod-shaped precipitates and the elongated second phase in Zr-1Nb heat-treated above the monotectoid temperature were $(NbFe)_2$ and β_{Zr} phase, respectively. It is interesting to note that the shape and structure of precipitates are different for Zr-1.1Nb-0.05Cu alloys with different heat treatment. The volume fraction of second phase precipitates appears to be increased by annealing and rapid cooling in the present study as shown in Fig. 1. The effect of initially different precipitates on the creep behavior is not likely to be appreciable in the annealed and stress-relieved Zr-1.1Nb-0.05Cu cladding tubes because the solubility of Nb increases to 0.45~0.50 wt% and significant fraction of precipitates are dissolved in the temperature range of creep testing (450~500 °C). Furthermore, the rod-shaped precipitates formed at 700 °C during annealing transforms to round shaped precipitates in the temperature range of creep testing at 450~500 °C [6].

Figure 2(a) and 2(b) display the creep curves of Zr-1.1Nb-0.05Cu cladding tubes at 500 °C, 475 °C and 450 °C; stress-relieved (a) and annealed (b). Both stress-relieved and annealed Zr-1.1Nb-0.05Cu alloys show normal creep curves consisting of primary, steady-state and tertiary regions although annealed specimen show inappreciable primary creep. It is interesting to note that the creep rate decreased significantly in the annealed Zr-1.1Nb-0.05Cu cladding tubes compared to those of stress-relieved Zr-1.1Nb-0.05Cu cladding tubes in the stress range of the present study. It should be emphasized that the steady-state creep rate became slower as well as the creep life was extended in the annealed Zr-1.1Nb-0.05Cu compared to those of the stress-relieved Zr-1.1Nb-0.05Cu. For example, the annealed Zr-1.1Nb-0.05Cu fractured after 108 hrs at 500 °C, 100 MPa whereas the Zr-1.1Nb-0.05Cu cladding tubes with

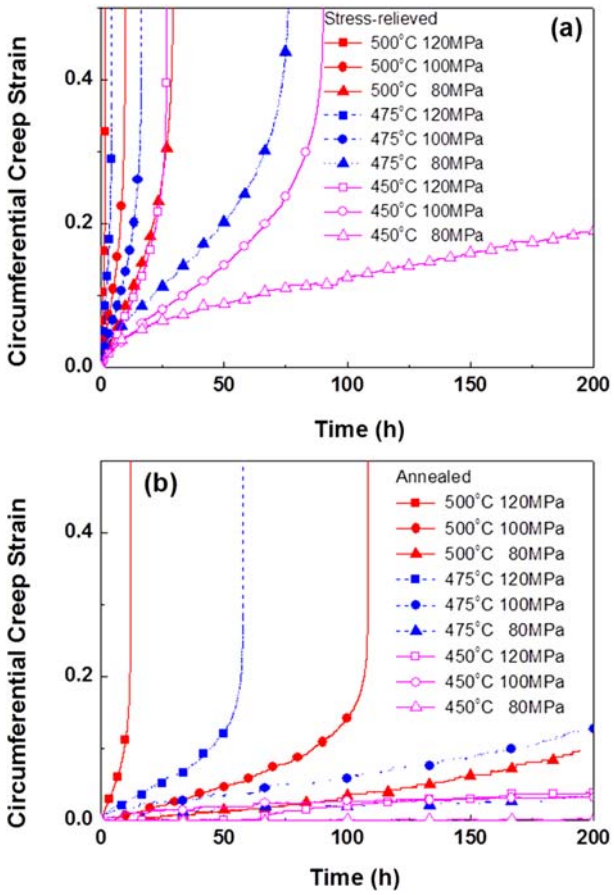

Fig. 2. Creep curves of stress-relieved (a) and annealed (b) Zr-1.1Nb-0.05Cu.

stress-relief treatment fractured only after 9.8hrs at the same temperature and load. The creep lives of annealed Zr-1.1Nb-0.05Cu alloy was extended over Zr-1.1Nb-0.05Cu alloy with stress-relief treatment by the factor of 6~15.

It has been reported that, in the temperature region where diffusional creep is predominant, the creep rate increases with the decrease of grain size because of the increasing fraction of the fast diffusion path along grain boundaries. Dislocation creep processes, on the other hand, have been considered to be independent of the grain size [13]. In the temperature region of dislocation creep, the creep rate is grain-size-insensitive in aluminum [13]. Other researchers have reported that the steady state creep rate may decrease or increase with increasing grain size, or be grain-size-independent in copper [13]. It has been reported that the creep rate reached to a minimum rate in the grain size range of 80-130 μm [16] and then increased with further increase of grain size in 316L stainless steel.

Lee *et al*. [16] reported that the observation of creep rate dependent on the grain size can be explained reasonably in terms of the model of Garofalo in which grain boundaries behave simultaneously as both barriers to dislocation motion and dislocation sources. The grain boundaries of they behave as barriers would decrease the creep rate but, if they behave as dislocation sources, grain boundaries would sometimes accelerate the creep rate [16]. The creep rate is known to be proportional to the square of grain size at intermediate temperatures in Cu and Cu alloys. The high temperature creep rate of Pb is reported to be inversely proportional to the grain size. It has been suggested by Wilshire and Palmer [13] that the steady state creep rate increases with the decrease of grain size because of the increasing contribution of recovery and rearrangement of dislocations within the boundary area with decrease of grain size. In both models, the influence of grain size on creep rate varies with the change of temperature and loading condition even in same material. The creep rate can be increased in the small grain size region because of increasing volume fraction of near-grain-boundary region if the dislocation activity increases in the near-grain-boundary regions. These models support the increase of creep rate with the decrease of grain size in the present study.

Figure 3, the creep rates of stress-relieved and annealed Zr-1.1Nb-0.05Cu at 450, 475, and 500 °C are plotted as a function of the stress. Compatible with the observation in

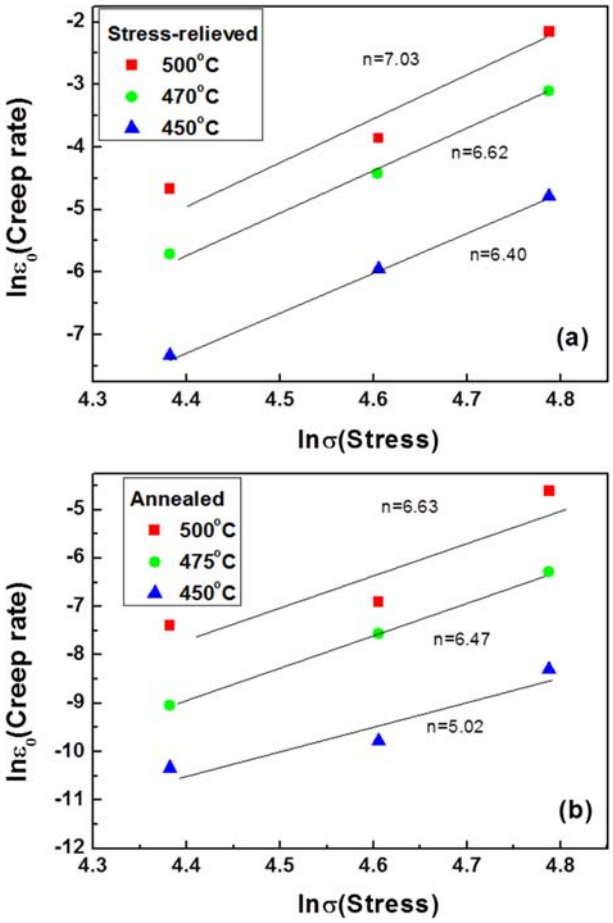

Fig. 3. Relationship between steady state creep rate and stress for stress-relieved (a) and annealed (b) Zr alloy at 450, 475, and 500 °C.

Fig. 2, the steady-state creep rates of Zr-1.1Nb-0.05Cu alloy tubes with annealing are significantly lower than those of Zr-1.1Nb-0.05Cu alloy with stress-relief heat-treatment. The creep rates decrease as the grain size increased with annealing. The stress exponents for creep increased slightly with the increase of temperatures in both alloys regardless of grain size. The stress exponents for creep of both stress-relieved and annealed Zr-1.1Nb-0.05Cu were observed to be 5~7, suggesting that the rate controlling creep mechanism is the dislocation climb in the present study [1]. Ruano *et al*. [17] suggested that, when the contribution of pipe diffusion is significant, the stress exponent increases by a factor of 2 over that obtained when lattice diffusion is dominant. The stress exponents (5~7) higher than that (=5) typically observed in the climb-controlled creep may be associated with the greater contribution of pipe diffusion along dislocation cores.

The activation energy for creep in stress-relieved Zr-1.1Nb-0.05Cu cladding tube in Fig. 4(a) was observed to be in the range of between 210~250 KJ/mole whereas that of annealed Zr-1.1Nb-0.05Cu alloy tube was found to be 250~340 KJ/mole (Fig. 4(b)). The activation energy for creep observed in this study is similar to those of creep for Zircaloy-2 (245-287 kJ/mol [18]) and Zr (234-271 kJ/mol [19]). The activation energy of creep increased appreciably in the annealed Zr-1.1Nb-0.05Cu alloy compared to those of stress-relieved alloy. Perez *et al*. [20] reported that the activation energy for self-diffusion below 600 °C is 336 KJ/mole. Interestingly enough, the highest activation energy calculated at low stress was close to 336 KJ/mole.

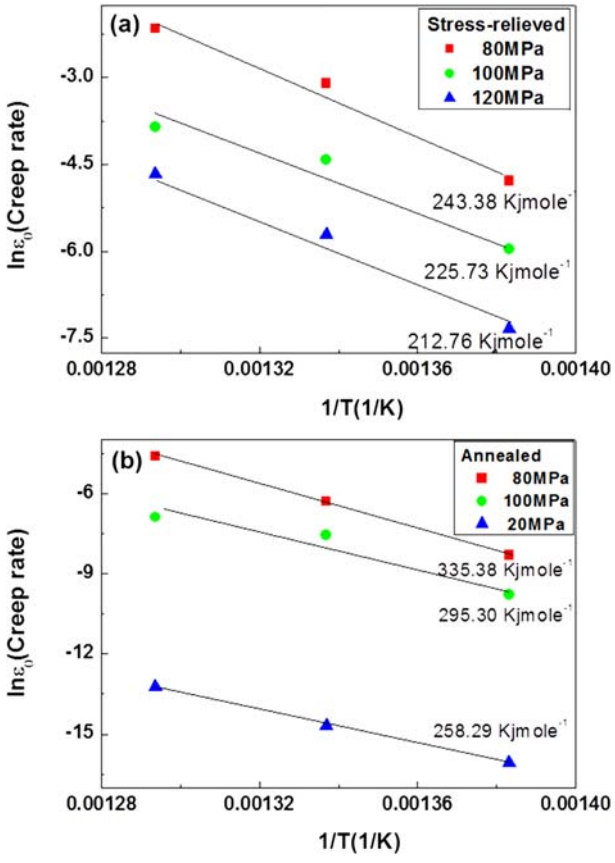

Fig. 4. Stead-state creep rate plotted against the reciprocal of temperature for stress-relieved (a) and annealed (b) Zr alloy at 450, 475 and 500 °C.

The increase of activation energy in the annealed Zr-1.1Nb-0.05Cu alloy is attributed to the decreasing contribution of faster diffusion path such as grain boundaries and dislocations. With the increase of grain size with annealing, the activation energy for creep increased as shown in Fig. 4. It has been generally believed that the diffusion activation energy for short-cut path such as dislocations and grain boundaries are 50~60% of those of lattice diffusion [17,21]. Since the activation energy for grain boundary diffusion is lower than that of lattice diffusion, the grain boundary diffusion definitely contribute to the creep deformation if the diffusion creep is dominant creep deformation mechanism [13]. Accordingly, the creep rate increases with decrease of grain size because of increasing contribution of grain boundary diffusion. The dislocation creep is also influenced by diffusion for both climb and glide controlled creeps [17,21,22]. Since the rate controlling mechanism of Zr-1.1Nb-0.05Cu alloy is climb controlled creep in the present study, the climb rate can also be influenced by grain size if the climb rate is enhanced by the stress concentration in pile-ups near grain boundaries [23] or aided by easier diffusion path along dislocations and grain boundaries [17,21].

Figuere 5(a) and 5(b) displays the TEM microstructure of stress relieved (a) and annealed (b) Zr-1.1Nb-0.05Cu creep-tested at 450 °C at the applied stress of 100 MPa. Grains with arrays of high dislocation density (indicated by black arrows) were observed in the stress-relived specimen after creep testing in Fig. 5(a). In Fig. 5(b), dislocation arrays (indicated by thick black arrows) were also observed. The dislocation density in the stress-relieved alloy is much higher, supporting the higher population of easier diffusion paths in the stress-relived alloy. The lower activation energy and higher creep rate in the stress-relived Zr-1.02Nb-0.69Sn-0.12Fe is supported by the presence of dislocation arrays with high

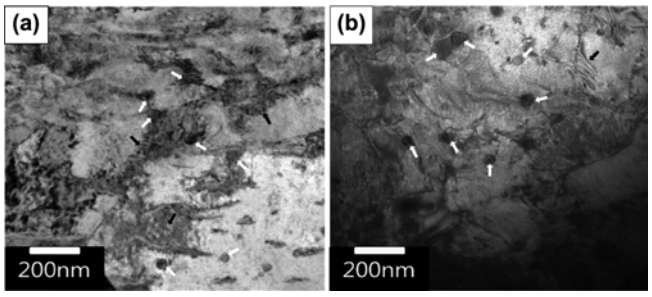

Fig. 5. TEM microstructure of stress relieved (a) and annealed (b) Zr-1.1Nb-0.05Cu creep-tested at 450 °C at the applied stress of 100 MPa.

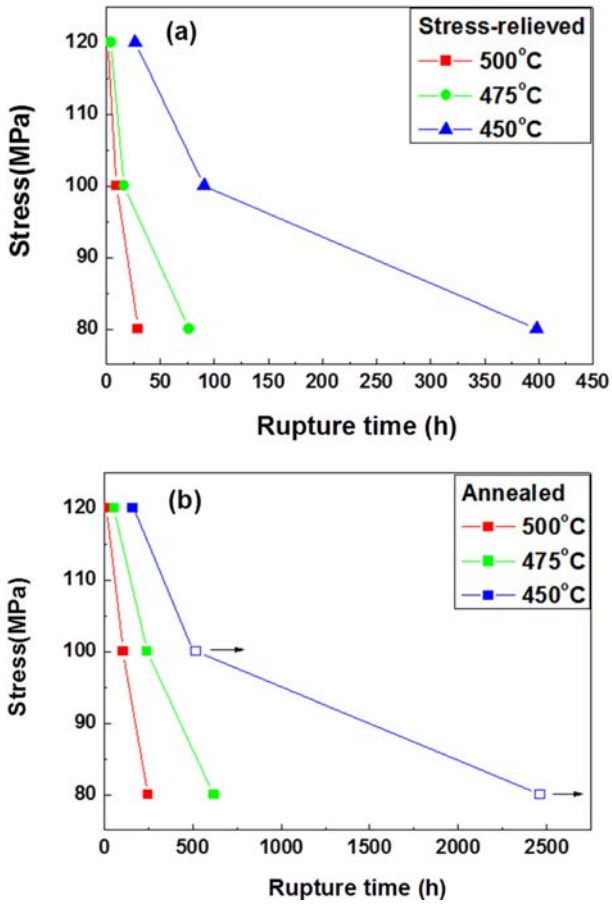

Fig. 6. Creep rupture time plotted against the stress for the stress-relieved (a) and annealed (b) Zr-1.1Nb-0.05Cu alloy.

dislocation density. The population and shape of precipitates (indicated by white arrows) in the annealed alloy after creep testing appeared different from those observed in the annealed alloy before creep testing. The rod-shaped precipitates transformed to the round shaped precipitates during creep testing. The creep behavior is not likely to be appreciably modified by initially observed precipitations just after annealing because the most precipitates are modified and/or dissolved during creep testing at 450~500 °C.

In Fig. 6(a) and 6(b), the time to creep fracture is plotted against the stress for the stress-relieved and annealed Zr-1.1Nb-0.05Cu alloy, respectively. As shown in these figures, creep life decreases with the increase of temperature and stress. It should be noted that the rupture time increased dramatically in the annealed Zr-1.1Nb-0.05Cu alloy compared to that of stress-relieved Zr-1.1Nb-0.05Cu alloy. For example, the rupture time of annealed Zr-1.1Nb-0.05Cu alloy crept at 450 °C and 80 MPa was ~2500 h whereas that of stress-relieved Zr-1.1Nb-0.05Cu alloy crept under the same temperature and stress conditions were ~400 h. In the same way, the rupture time of annealed Zr-1.1Nb-0.05Cu alloy crept at 500 °C and 80 MPa was ~250 h whereas that of stress-relieved Zr-1.1Nb-0.05Cu alloy crept under the same temperature and stress conditions was ~30 h. In Fig. 6(a), the open squares and horizontal arrows for the creep of annealed Zr-1.1Nb-0.05Cu alloy at 450 °C indicates that the creep tests were stopped before fracture at the points where the open squares were placed. Therefore, the rupture time would be much longer than those indicated by open squares at 450 °C.

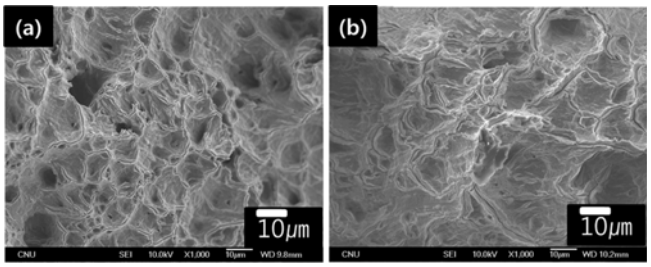

Fig. 7. SEM fracture surface image of Zr-1.1Nb-0.05Cu crept at 100 MPa and 500 °C: (a) stress-relieved Zr alloy and (b) annealed Zr-alloy.

Figure 7(a) and 7(b) showed the SEM images of fracture surfaces of stress-relieved and annealed Zr alloy creep-tested at 100 MPa and 500 °C. In both creep-fractured specimens, the ductile fracture surfaces were observed as represented by dimples on the fracture surface. The dimple size of annealed Zr-1.1Nb-0.05Cu alloy was found to be greater than that of stress-relieved Zr-1.1Nb-0.05Cu alloy, compatible with the coarse microstructure and grain size in the annealed Zr-1.1Nb-0.05Cu alloy. In the annealed Zr-1.1Nb-0.05Cu alloy, some secondary cracks were observed along the grain boundaries on the creep-fractured surface [24]. The presence of the secondary crack in the annealed Zr-1.1Nb-0.05Cu alloy can be attributed to the much longer creep life. With the increase of creep life, the total number of thermal vacancies moved to or captured at grain boundaries increases [25], causing the formation of voids or interconnected cracks at grain boundaries.

4. CONCLUSIONS

Creep properties of annealed and stress-relieved Zr-Nb-Cu alloys were investigated in the present study and the important findings are as follows;

(1) The stress exponents for creep of annealed and stress-relieved Zr-1.1Nb-0.05Cu were observed to be 5~7, suggesting that the rate controlling creep mechanism is the dislocation climb.

(2) The activation energy for creep of Zr-Nb-Cu alloys was observed to be close to those of creep for Zircaloy-2 (245-287 kJ/mol) and Zr (234-271 kJ/mol).

(3) The activation energy for creep increased appreciably in the annealed Zr-1.1Nb-0.05Cu alloy compared to those of stress-relieved alloy. The increase of activation energy in the annealed Zr-1.1Nb-0.05Cu alloy is attributed to the

decreasing contribution of faster diffusion path such as grain boundaries and dislocations.

(4) The creep rate at intermediate temperatures decreased with the increase of grain size in the annealed Zr-1.1Nb-0.05Cu, implying the creep resistance can be improved by the increase of grain size.

(5) The creep lives of annealed Zr-1.1Nb-0.05Cu also increased over the stress-relieved Zr-1.1Nb-0.05Cu, supporting the enhancement of the creep resistance of Zr-1.1Nb-0.05Cu with increasing grain size in the intermediate temperature region of dislocation-based creep.

ACKNOWLEDGMENT

The authors are grateful for the support from the Fundamental Research and Development Program for Industrial Technology, funded through the Ministry of Trade, Industry and Energy (2014).

REFERENCES

1. S. Y. Lee, K. T. Kim, and S. I. Hong, *J. Nucl. Mater.* **392**, 63 (2009).
2. S. Ko, S. I. Hong, and K. T. Kim, *J. Nucl. Mater.* **404**, 154 (2010).
3. S. L. Mannan and P. Rodriguez, *Mater. Sci. Technol*. **17**, 63 (1983).
4. R. A. Holt and A. R. Causey, *J. Nucl. Mater.* **335**, 529 (2004).
5. W. N. Kim, Y. Choi, and S. I. Hong, *Phys. Metals Metallogr.* **13**, 1313 (2014).
6. Y. H. Jeong, H. G. Kim, and T. H. Kim, *J. Nucl. Mater.* **317**, 1 (2003).
7. J. J. Won, S. J. Min, and K. T. Kim, *Met. Mater. Int.* **21**, 31 (2015).
8. Y. I. Jung, J. Y. Park, and Y. H. Jeong, *Met. Mater. Int.* **17**, 15 (2011).
9. S. Ko, S. I. Hong, K. T. Kim, and Y. H. Jeong, *J. Nucl. Mater.* **414**, 138 (2011).
10. G. B. Jeong, Y. Choi, and S. I. Hong, *Phys. Metals Metallogr.* **115**, 1281 (2014).
11. S. I. Hong, K.W Lee, and K.T Kim, *J. Nucl. Mater.* **303**, 169 (2002).
12. S. I. Hong and K.W. Lee, *J. Nucl. Mater.* **340**, 203 (2005).
13. B. Wilshire and C. J. Palmer, *Scr. Mater.* **46**, 483 (2002).
14. Y. N. Seol, Y. I. Jung, B. K. Choi, J. Y. Park, and S. I. Hong, *Kor. J. Met. Mater.* **49**, 355 (2011).
15. D. Gloaguen, T. Berchi, E. Girard, and R. Guille, *J. Nucl Mater.* **374**, 138 (2008).
16. Y. S. Lee, D. W. Kim, D. Y. Lee, and W. S. Ryu, *Met. Mater. Int.* **7**, 107 (2001),
17. O. A. Ruano, A. K. Miller, and O. D. Sherby, *Mater. Sci. Eng.* **51**, 9 (1981).
18. D. O. Northwood, X. Meng, and B. O. Warr, *ASTM STP.* **1132**, 156 (1991).
19. J. J. Holmes, *J. Nucl Mater.* **13**, 137 (1964).
20. R. A. Perez1, H. Nakajima, and F. Dyment, *Mater. Trans.* **44**, 2 (2003).
21. S. W. Nam, S. I. Hong, and D. H. Shin, *J. Mater. Sci.* **18**, 1743 (1983).
22. S. I. Hong, *Mater. Sci. Eng.* **82**, 175 (1986).
23. S. I. Hong, *Mater. Sci. Eng.* **76**, 77 (1985).
24. E. K. Lee and S. I. Hong, *Korean J. Met. Mater.* **51**, 15 (2013).
25. J. S. Lee and K. Maruyama, *Met. Mater. Int.* **21**, 639 (2015).